A COMPUTATIONAL FRAMEWORK FOR EARLY-STAGE EVTOL CRASHWORTHINESS EVALUATION

Edoardo Novembre
Politecnico di Milano
Milan, Italy

Sebastiano Di Mauro
Politecnico di Milano
Milan, Italy

Paolo Astori
Politecnico di Milano
Milan, Italy

Alessandro Airoldi
Politecnico di Milano
Milan, Italy

ABSTRACT

This work presents a numerical methodology aimed at supporting the early-stage crashworthiness evaluation of eVTOL aircraft. A simplified simulation framework combining finite element and multi-body modeling was developed to enable fast exploration of a broad design space with limited computational effort. A two-step design of experiments supported by surrogate modeling allowed for the identification of feasible design regions and the quantification of parameter influence through Sobol' sensitivity indices. The results reveal that tuning the different energy-absorbing components to ensure a synergistic system response plays a central role in minimizing lumbar load peaks while avoiding seat bottoming. Notably, a compliant subfloor benefits both occupant survivability and the loads experienced by the airframe and the battery pack. These findings underscore the importance of integrating crashworthiness criteria from the earliest stages of eVTOL structural design and demonstrate the potential of the proposed approach to provide requirements that can guide design decisions.

INTRODUCTION

As sustainability-driven innovation becomes increasingly central, battery-based electric vehicles are one of the most investigated solutions for the next generation of aircraft. Among them, all-electric and hybrid-electric Vertical Take-Off and Landing (eVTOL) aircraft stand out, being considered as promising candidates for Air Metro and Air Taxi services within Urban Air Mobility projects.

As with all innovative technologies and configurations, safety is a key concern for manufacturers, aviation agencies, and passengers (Ref. 1). For eVTOLs, the challenge is made even more complex by the expected low-altitude and constrained airspace operations, which might occur within the statistically less safe on-demand model (Ref. 2). As a result, a successful eVTOL design should include crashworthiness as core design factor. The study presented in (Ref. 3) identified some primary crashworthiness requirements including mass retention, occupants loads, and survivable volume. In addition, it defined secondary requirements that are peculiar of eVTOLs, such as battery safety, multi-terrain and unlevelled impact conditions. Given the broad range of possible crash scenarios and the high cost of full-scale crash tests (Ref. 4), researchers are focusing on developing numerical tools to assess the crash performance of eVTOL aircraft (Refs. 3, 5–7).

The work presented in (Ref. 8) highlights how thorough material characterization and component testing are essential to guarantee accurate prediction capability under the complex dynamic loading conditions typical of real-world crash events. Such complexity often leads to unpredictable and suboptimal performance of energy-absorbing components that, while performing well under nominal and controlled testing conditions, fail to behave as expected in full-scale tests (Ref. 9). Given these considerations, it becomes essential to adopt a system-level crashworthiness approach (Ref. 10) that can consider the broad range of possible crash scenarios and interactions between energy-absorbing components.

The aim of this paper is to present a numerical approach for investigating the crash performance of an eVTOL aircraft during its early design phase, when there is a need to explore a large design space and limited experimental data availability. This is accomplished through Finite Element (FE) analyses that make extensive use of lumped connector elements and rigid bodies to gain computational efficiency. The objective of the proposed framework is therefore to highlight trends and rules of thumb considering three main crashworthiness criteria: occupants' loads, battery deceleration and the loads acting on the airframe.

Even with the simplifications introduced in the model, the numerical strategy, coupled with Gaussian process regression (GPR) (Ref. 11), proves useful for capturing key trends and performing meaningful exploration of the variable space. To illustrate this, results will be presented considering a reference cabin configuration and a 8 m/s vertical drop test on rigid ground simulated with the Abaqus/Explicit solver.

KEY FEATURES OF THE MODEL

ATD and seat

To evaluate occupant loads, the model includes an Anthropomorphic Test Device (ATD) and a Martin-Baker seat. Both the ATD and the seat are idealized as rigid bodies connected by joints, with some exceptions. In particular, the lumbar spine of aeronautical Hybrid III 50th percentile male dummy is modeled using deformable solid elements, as this region is critical for accurately reconstructing the lumbar load injury criterion during the crash simulation. Moreover, the components involved in the contact between the base and backrest of the seat and the ATD are modeled using deformable finite elements. Particular care was taken in assigning appropriate contact definitions and in selecting a suitable hyperfoam material model for the dummy's jacket, thigh, and pelvic regions. Finally, the seat belts are simply represented by beam elements. The remaining rigid parts of the dummy are connected using connector elements available in the Abaqus library and interact through defined surface interactions. The crashworthy seat is modeled as two rigid sliding components, namely the seat bucket and the trucks, connected by a spring element exhibiting an elastic–plastic response with a final bottoming phase.

This model was mainly developed and validated against experimental data in previous work (Ref. 12). Two key metrics were used to assess its accuracy: the peak lumbar load observed during the initial impact phase, and the occurrence of bottoming. This is motivated by the fact that the simplified model cannot reliably capture the post-bottoming response. As a result, bottoming events are treated as failures, just like cases where the lumbar load exceeds the limit prescribed by regulations. The good agreement between numerical and experimental results, shown in Figure 1, points out that the ATD and seat model can be considered reliable tools, especially in light of their computational efficiency (3 minutes with a single processor). In this case, the seat stroke was limited to 120 mm due to operational requirements.

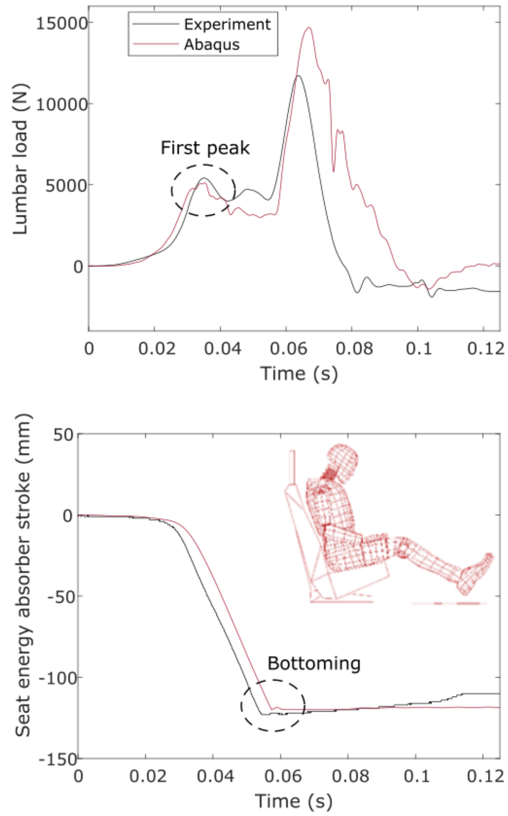

Figure 1. ATD and seat models validation.

Airframe and subfloor model

In this work, the cabin model of a tilt-rotor eVTOL with four passengers and one pilot is used as the reference test configuration. The airframe is modeled using beam and shell elements with an average element size of 30 mm. This mesh size was selected following a sensitivity study, in which meshes with element sizes of 20, 30, 45, and 60 mm were compared. The lumbar load response of dummies was chosen as the reference metric to ensure that the perceived impact kinematics were not significantly affected by mesh dependency. With a 30 mm mesh size, the normalized Root Mean Square Error (RMSE) with respect to the finest mesh remains below 3% for all ATDs.

The material properties of a carbon-fibre-reinforced-plastic (CFRP) fabric, including the damage model described in (Ref. 6), are assigned to the skin, while the frames are modeled as fully elastic. This modeling choice is motivated by the fact that the simplified model is not intended to predict airframe failure mechanisms, but rather to reproduce reasonable occupant loads and provide insight into the loads experienced by the frame. The structure was sized primarily based on the emergency landing load requirements specified in CS § 27.561, as well as on typical panel and frame size reported in the literature for VTOL vehicles (Refs. 6, 13, 14).

Two battery packs are included in the cabin: one mounted on the upper frame near the center wing section, and the other located in the aft fuselage. The battery packs are modeled as rigid bodies and connected to the airframe via Multi-Point Constraints (MPCs). Their purpose is twofold: to account for the inertial contribution of the batteries in the crash simulations, and to enable the measurement of the macroscopic deceleration experienced by the packs during the impact. The upper battery pack has a mass of 150 kg, while the aft pack weighs 200 kg. It is assumed that the remaining battery cells required to meet the total energy demand are installed within the wingbox.

Finally, the subfloor is modeled using a different approach: the skin connecting the floor to the underfloor is removed, and the two components are linked through a large number of connector elements exhibiting an elastic–perfectly plastic behavior. These elements are intended to represent the contribution of energy absorbers (EAs), which are commonly integrated into crashworthy subfloors to dissipate energy through progressive crushing. The distribution of these connectors will be discussed in detail in the following subsection.

Parametrization and metrics

The subfloor connectors are organized into sets, as illustrated in Figure 2. Referring to a typical subfloor structure composed of keel beams, transverse bulkheads, and intersection elements (Ref. 13), the connectors are classified as follows: passengers' (light blue) and pilot's (green) intersection elements; passengers' (dark grey) and pilot's (grey) intermediate elements; and front (orange), middle (blue), and rear (red) frame elements. This setup can represent traditional EA placement configurations and account for the structural reinforcement that are found at the main frames. The yielding force (F^Y) of the connectors was parameterized within a tentative design space for an exploratory Design of Experiments (DOE). Additionally, the yielding force of the seat absorber was included as a design parameter. The preliminary bounds defining the design space are listed in Table 1.

The performance of the EA configurations are evaluated using the following metrics: the lumbar load of the pilot, one front passenger, and one rear passenger; the section forces measured by virtual load cells placed on the main frames; the deceleration of the upper battery pack; and the stroke of the seats. The aft battery pack was not considered, as its low position—close to highly deformed elements—led to high acceleration spikes that were largely uncorrelated with the subfloor design. The selected metrics are summarized in Figure 3.

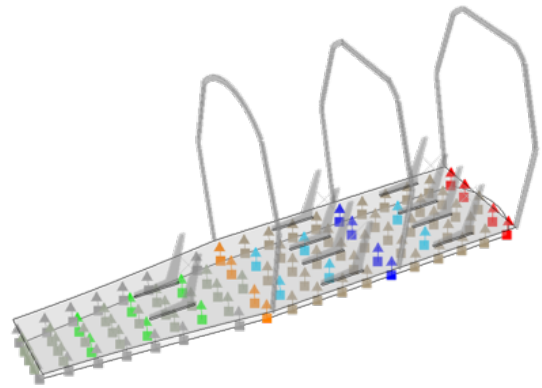

Figure 2. Subdivision into sets of the subfloor absorbers.

Table 1. EA Elements Preliminary Design Space

EA element	Min. F^Y (kN)	Max. F^Y (kN)
Intermediate pass.	0.1	1.5
Intermediate pilot	0.1	2.5
Front frame	6.0	45.0
Middle frame	6.0	45.0
Rear frame	6.0	30.0
Intersection pass.	6.0	24.0
Intersection pilot	6.0	24.0
Seat absorber	8.0	16.0

EXPLORATORY DOE

The design space presented in Table 1 was sampled using the Latin Hypercube Sampling (LHS) technique, generating a total of 150 design points. Each simulation required approximately 2 hours and 30 minutes using 20 processors. The main objective of this exploratory DOE was to identify more meaningful variable ranges, i.e. regions of the design space with a high density of configurations in which all occupants remained below the lumbar load limit and no seat bottoming occurred. However, this condition was met in only one out of the 150 simulated configurations.

The analysis of the outcomes leads to two main considerations: (i) within these ranges, the seat absorber force is by far the key driver; (ii) ensuring the survivability of both the passengers and the pilot appears to be feasible only within a very narrow portion of the design space.

Since limited additional information could be directly extracted to refine the bounds of the variables, a predictive tool based on GPR trained on the already available samples was developed to explore new design points without requiring further computationally expensive FE simulations.

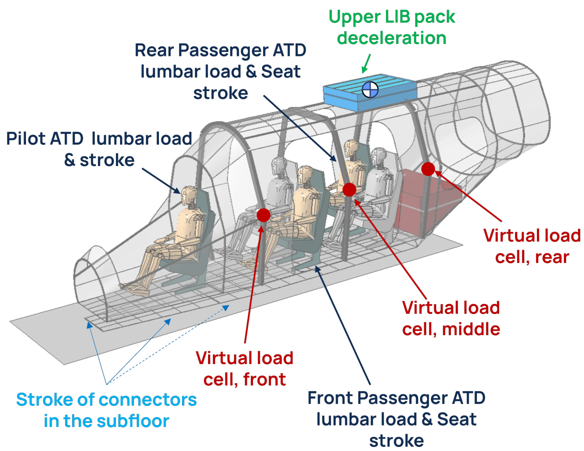

Figure 3. eVTOL configuration and metrics.

Identification of new bounds with GPR

Gaussian process regression is a non-parametric approach used to predict an output y at unsampled input locations, based on a set of observed input–output pairs (X, y). In addition to the predicted mean output, GPR also provides a standard deviation that quantifies the uncertainty of the prediction at each input location (Ref. 11).

If the lumbar load l^i and seat stroke s^i, where i refers to the i-th dummy, are treated as black-box functions of the EA parameters $\mathbf{x}$, they can be approximated using Gaussian Processes, as shown in Eq. 1.

$$l^i(\mathbf{x}), s^i(\mathbf{x}) \sim GP(m^i(\mathbf{x}), k^i(\mathbf{x}, \mathbf{x}')) \tag{1}$$

where $m^i(\mathbf{x})$ and $k^i(\mathbf{x}, \mathbf{x}')$ are the mean and the covariance functions of the i-th process (Ref. 11). The sum of a Matérn 5/2 kernel and a WhiteKernel from the *scikit-learn* (Ref. 15) library was selected as the covariance function. The exploratory DOE data was then used to fit a GPR model for the peak lumbar load during the initial impact phase and the used seat stroke of the three considered ATDs.

The true vs. predicted plots evaluated on test points, i.e. data from the exploratory DOE not used during GP training, showed R^2 scores ranging from 0.92 to 0.99. This indicates that the predictor is accurate enough to reliably explore the design variable ranges. The conditions expressed in Eq. 2 define what is considered as a feasible point.

$$\begin{cases} l^i(\mathbf{x}) < 6670 = \bar{l} & i = 1,2,3 \\ s^i(\mathbf{x}) < 185 = \bar{s} & i = 1,2,3 \end{cases} \tag{2}$$

Actually, the GPR uncertainty was taken into account by considering both the predicted mean μ and the associated standard deviation σ at each point $\mathbf{x}^0$. As shown in Eq. 3, the constraints were formulated in probabilistic terms by using the normal cumulative distribution functions $\Phi^i_{l,s}$.

$$\begin{cases} \prod_{i=1}^{3} \Phi^i_l \left(\dfrac{\bar{l} - \mu^i_l(\mathbf{x}^0)}{\sigma^i_l(\mathbf{x}^0)} \right) > 0.95 \\ \prod_{i=1}^{3} \Phi^i_s \left(\dfrac{\bar{s} - \mu^i_s(\mathbf{x}^0)}{\sigma^i_s(\mathbf{x}^0)} \right) > 0.95 \end{cases} \tag{3}$$

By evaluating the constraints defined in Eq.3 over a large number of points within the design space, new feasible ranges were identified. These updated ranges, reported in Table2, will be used in the subsequent DOE and can be compared with those in Table 1.

Table 2. New Ranges Identified Through GPR

EA element	Min. F^Y (kN)	Max. F^Y (kN)
Intermediate pass.	0.1	1.0
Intermediate pilot	0.1	1.0
Front frame	2.5	12.0
Middle frame	20.0	30.0
Rear frame	2.5	12.0
Intersection pass.	1.0	6.0
Intersection pilot	1.0	6.0
Seat absorber	9.5	10.5

Some interesting considerations can be drawn: (i) feasible points generally occur when the EA forces are near the lower bounds of the initial design space; (ii) among the subfloor EAs, the middle frame is the only one that requires relatively high force values; (iii) the admissible range for the seat force is significantly narrowed, which aligns with its strong influence observed in the exploratory DOE; (iv) it was verified that the reduced range for the seat force complies with CFR § 27.562. Figure 4 illustrates the distribution of feasible points for selected variables, which was the basis for the definition of the design space ranges for the DOE presented in the next section.

RESULTS OF THE REFINED DOE

For the new DOE, a total of 200 simulations were run within the design space presented in Table 2. Remarkably, about 20% of the configurations resulted in survivable outcomes, highlighting the effectiveness of the procedure described in the previous section. However, the simulations generated a large amount of data, making it difficult to extract meaningful insights. To address this, a sensitivity analysis based on Sobol' indices was performed.

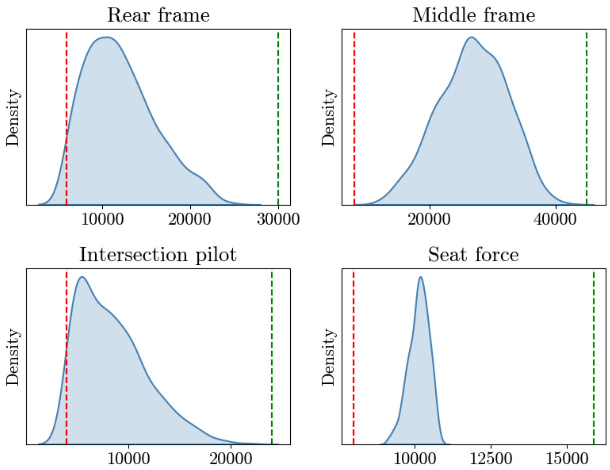

Figure 4. Distribution of feasible points for selected variables.

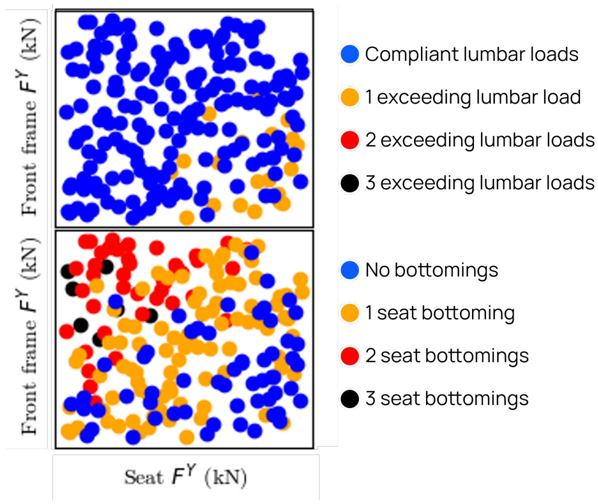

Figure 5. Survivable configurations.

Sobol' analysis

Sobol' sensitivity analysis can be used to quantify how much the global variance of a given function depends on each of its inputs. In this case, the objective is to evaluate which are the EAs parameters that mostly impact the metrics depicted in Figure 3. Two indices are considered: the first-order index, which quantifies the effect of an input variable alone, and the total-effect index, which captures the overall contribution of an input, including all higher-order interactions with other variables (Ref. 16).

Since computing Sobol' indices requires a large number of function evaluations, the 200 samples were again used to fit GPR models. The resulting R^2 scores ranged between 0.80 and 0.96. Although the GPR models may not always be suitable for accurately predicting exact values, they are sufficiently reliable to capture the overall trends in the problem, which is the primary goal of this sensitivity analysis.

The *SAlib* library was used to compute Sobol' indices (Ref. 17). A selection of the first order Sobol' indices for each class of the considered metrics is reported in Figure 3.

It is apparent that both the first lumbar load peak and the seat stroke are strongly influenced by the response of the frontal frame connectors, despite their primary structural role not being energy absorption. It is also worth noting that the values of the Sobol' indices depend on the chosen parameter bounds. This is illustrated by the fact that narrowing the range of the seat absorber significantly reduced its influence on both the lumbar load and the maximum stroke. Before this reduction, the Sobol' indices associated with the seat absorber were about 0.7 for these metrics.

Another insight is that the loads experienced by the frame can be mitigated not only by modifying the response of the elements directly beneath it, but also by tuning the strength of energy-absorbing components. A similar effect is also observed for the peak deceleration of the upper battery pack, whose integrity is a critical aspect to consider.

Analysis of the results

First, the survivable configurations are shown in Figure 5, with the seat absorber force and the yielding force of the front frame connector on the axes. The scatter plot highlights that, within the new parameter ranges, the first peak of lumbar load is almost always below the allowable maximum. The few configurations where the lumbar load limit is exceeded always involve the pilot. In contrast, avoiding seat bottoming appears to be more challenging.

Analyzing the results, it emerges that when the connector of the front frame is too strong, almost all configurations lead to bottoming of at leat one of the seats. On the other hand, solutions with a lower yielding force are able to prevent bottoming in most cases, but if the seat absorber force is too high, the lumbar load of the pilot may exceed the regulatory limit. This highlights the need to calibrate the response of the subfloor and the seat so that they can effectively work as a system. Figure 6 shows the ratio between the subfloor force beneath the pilot and the force of the pilot's seat absorber plotted against the lumbar load peak and the utilized seat stroke. A ratio of approximately 1.5 is found to produce most of the successful configurations.

Finally, the metrics related to the loads recorded by the virtual load cells and the deceleration of the battery pack are analyzed. The results show that lower strength values

Table 3. Outcomes of the Sobol' sensitivity analysis, selected metrics.

EA element	Lumbar load, front pass.	Seat stroke, front pass.	Load, rear virtual cell	Upper pack deceleration
Intermediate pass.	0.005	0.026	0.250	0.013
Intermediate pilot	0.015	0.007	-0.004	0.010
Front frame	0.447	0.481	-0.001	0.018
Middle frame	0.063	0.028	0.069	0.501
Rear frame	0.013	0.005	0.464	0.141
Intersection pass.	0.051	0.130	0.153	0.256
Intersection pilot	0.004	0.010	0.000	-0.001
Seat absorber	0.230	0.254	-0.003	0.018

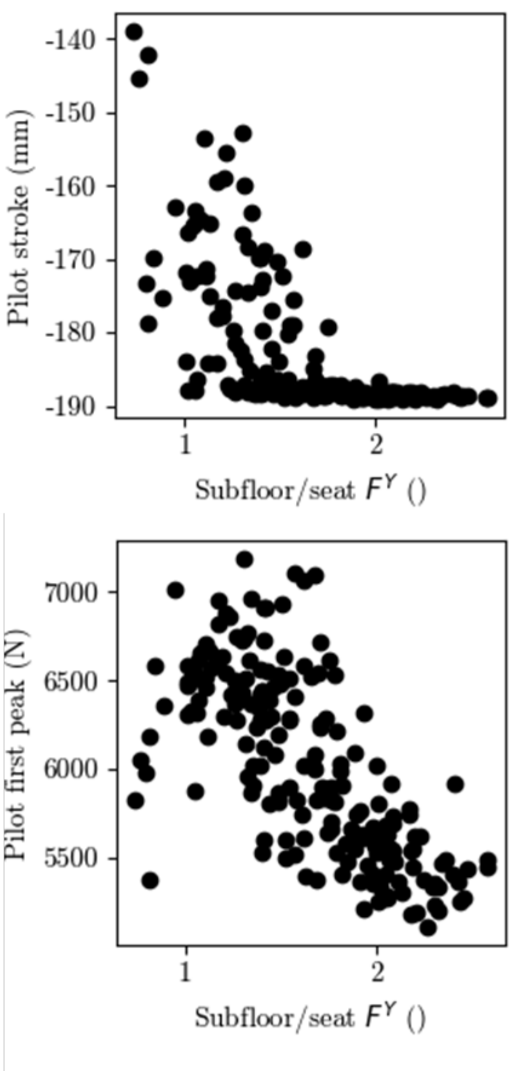

Figure 6. Relevance of the subfloor/seat ratio.

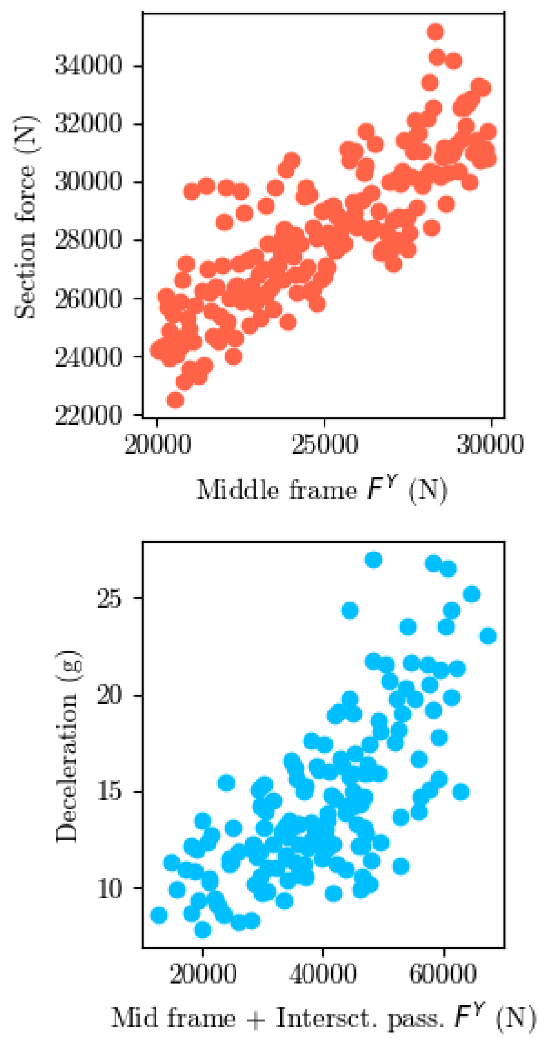

Figure 7. Effect of EAs on structural metrics.

for the connectors placed beneath the main frames are beneficial not only for the survivability of the occupants, but also for reducing structural loads and the deceleration experienced by the upper battery pack. For example, the section force in the middle frame can be reduced by up to approximately 30%, and the battery decelerations can be kept below the thresholds prescribed by UN38.3 *Test T.4: Shock*, that for the 150 kg Li-Ion battery pack would be 14.4 g. These outcomes are summarized in Figure 7.

CONCLUSIONS

This work led to the following key findings and remarks:

1. The simplified modeling approach, combining finite element and multi-body techniques, enabled the exploration of a wide design space with relatively limited computational effort, yielding relevant insights for the conceptual design and requirements of the subfloor.

2. Gaussian process regression proved to be an effective tool for defining feasible design ranges and performing sensitivity analyses, even when its predictive accuracy was not optimal. This is supported by the significant increase in the number of successful configurations found in the refined DOE, as well as by the Sobol' analysis results, which were consistent with the trends observed in the scatter plots.

3. A compliant subfloor was found to be highly beneficial from both survivability and structural perspectives. Moreover, the analysis revealed that different regions of the subfloor may require distinct calibrations of the energy absorbers and that the seat and the subfloor should be jointly designed to account for their mutual interaction. This underlines the importance of incorporating crashworthiness as a key design consideration from the early stages of eVTOLs' development.

Future work may involve investigating crash scenarios that incorporate forward velocity components and potentially soft soil conditions, in order to fully assess the capabilities of the proposed numerical approach in simulating real-world crash events.

Author contact:

Edoardo Novembre edoardo.novembre@polimi.it
Sebastiano Di Mauro sebastiano.dimauro@polimi.it
Paolo Astori paolo.astori@polimi.it
Alessandro Airoldi alessandro.airoldi@polimi.it

ACKNOWLEDGMENTS

This study was carried out within the MOST - Sustainable Mobility National Research Center and received funding from the European Union Next-Generation EU (Piano Nazionale di Ripresa e Resilienza (PNRR) - Missione 4. Componente 2, Investimento 1.4 - D.D. 1033 17/06/2022, CN00000023). This manuscript reflects only the authors' views and opinions, neither the European Union nor the European Commission can be considered responsible for them.

REFERENCES

1. Thomas Edwards and George Price. eVTOL passenger acceptance. Technical report, NASA, Ames Research Center, 2020.
2. Justin Littell. Challenges in vehicle safety and occupant protection for autonomous electric vertical take-off and landing (eVTOL) vehicles. In *AIAA Pro-pulsion and Energy 2019 Forum*, Indianapolis, IN, August 2019.
3. Matthias Waimer, Paul Schatrow, and Marius Lützenburger. Simulation studies on eVTOL crashworthiness in the conceptual and preliminary design phase. In *Tenth Triennial International Aircraft Fire and Cabin Safety Research Conference*, Atlantic City, NJ, October 2022.
4. Francesco Caputo, Giuseppe Lamanna, Donato Perfetto, Antonio Chiariello, Francesco Di Caprio, and Luigi Di Palma. Experimental and numerical crashworthiness study of a full-scale composite fuselage section. *AIAA Journal*, 59(2):700–718, 2021.
5. Menglong Ding, Anhuan Xie, Shiqiang Zhu, Wei Song, Jiandong Cai, Xufei Yan, Pengyu Zhao, Jason Gu, and Yanyan Zhang. Crashworthiness design optimization for an eVTOL aircraft. In *2022 IEEE International Conference on Robotics and Biomimetics (ROBIO)*, pages 82–86, 2022.
6. Jacob Putnam and Justin Littell. Crashworthiness of a lift plus cruise eVTOL vehicle design within dynamic loading environments. In *76th Vertical Flight Society's Annual Forum & Technology Display*, Virginia Beach, VA, October 2020.
7. Edoardo Novembre, Antonio Maria Caporale, Sebastiano Di Mauro, Paolo Astori, Chiara Mirani, and Alessandro Airoldi. Development of a multi-scale numerical approach for the crashworthiness of eVTOL aircrafts. In *50th European Rotorcraft Forum*, Marseille, France, September 2024.
8. Jacob Putnam and Justin Littell. Simulation and analysis of NASA lift plus cruise eVTOL crash test. In *Vertical Flight Society's 79th Annual Forum*, West Palm Beach, FL, May 2023.
9. Karen E. Jackson. Advances in rotorcraft crashworthiness: Trends leading to improved survivability. *Journal of the American Helicopter Society*, 63:021001, 2018.

10. Akif Bolukbasi. Full spectrum crashworthiness criteria for rotorcraft. Technical Report RDECOM TR 12-D-12, 2011.

11. Carl Edward Rasmussen and Christopher K. I. Williams. *Gaussian Processes for Machine Learning*. MIT Press, Cambridge, MA, 2006. Chapter 2.

12. Benedetta Cacchione, Alessandro Airoldi, and Paolo Astori. A hybrid modelling technique for the energy absorption capabilities of a crashworthy helicopter structure. In *37th European Rotorcraft Forum*, Gallarate, Italy, September 2011.

13. Chiara Bisagni. Crashworthiness of helicopter subfloor structures. *International Journal of Impact Engineering*, 27(10):1067–1082, 2002.

14. Kevin Hughes, Rade Vignjevic, and James Campbell. Experimental observations of an 8 m/s drop test of a metallic helicopter underfloor structure onto a hard surface: Part 1. *Proceedings of the Institution of Mechanical Engineers, Part G: Journal of Aerospace Engineering*, 221(5):661–678, 2007.

15. F. Pedregosa, G. Varoquaux, A. Gramfort, V. Michel, B. Thirion, O. Grisel, M. Blondel, P. Prettenhofer, R. Weiss, V. Dubourg, J. Vanderplas, A. Passos, D. Cournapeau, M. Brucher, M. Perrot, and E. Duchesnay. Scikit-learn: Machine learning in Python. *Journal of Machine Learning Research*, 12:2825–2830, 2011.

16. Toshimitsu Homma and Andrea Saltelli. Importance measures in global sensitivity analysis of nonlinear models. *Reliability Engineering & System Safety*, 52(1):1–17, 1996.

17. Jon Herman and Will Usher. SALib: An open-source python library for sensitivity analysis. *The Journal of Open Source Software*, 2(9), jan 2017.

CLASSIFICATION & COPYRIGHT